Author(s): Akola, Jaakko; Atodiresei, Nicolae; Kalikka, Janne; Larrucea, Julen; Jones, Robert O.

Title: Structure and dynamics in liquid bismuth and Bin clusters: A density functional study

Year: 2014

Version:

Please cite the original version:

Akola, J., Atodiresei, N., Kalikka, J., Larrucea, J., & Jones, R. O. (2014). Structure and dynamics in liquid bismuth and Bin clusters: A density functional study. Journal of chemical physics, 141(19), Article 194503. https://doi.org/10.1063/1.4901525

Structure and dynamics in liquid bismuth and Bi n clusters: A density functional study

J. Akola, N. Atodiresei, J. Kalikka, J. Larrucea, and R. O. Jones

Citation: The Journal of Chemical Physics **141**, 194503 (2014); doi: 10.1063/1.4901525
View online: http://dx.doi.org/10.1063/1.4901525
View Table of Contents: http://scitation.aip.org/content/aip/journal/jcp/141/19?ver=pdfcov
Published by the AIP Publishing

Structure and dynamics in liquid bismuth and Bi_n clusters: A density functional study

J. Akola,[1,2] N. Atodiresei,[3] J. Kalikka,[1,a)] J. Larrucea,[4,b)] and R. O. Jones[5,6,c)]
[1]*Department of Physics, Tampere University of Technology, P.O. Box 692, FI-33101 Tampere, Finland*
[2]*COMP Centre of Excellence, Department of Applied Physics, Aalto University, FI-00076 Aalto, Finland*
[3]*Peter Grünberg Institut PGI-1 and Institute for Advanced Simulation IAS-1, Forschungszentrum Jülich, D-52425 Jülich, Germany*
[4]*Nanoscience Center, Department of Physics, University of Jyväskylä, P.O. Box 35, FI-40014 Jyväskylä, Finland*
[5]*Peter Grünberg Institut PGI-1 and JARA/HPC, Forschungszentrum Jülich, D-52425 Jülich, Germany*
[6]*German Research School for Simulation Sciences, FZ Jülich and RWTH Aachen University, D-52425 Jülich, Germany*

(Received 5 June 2014; accepted 27 October 2014; published online 18 November 2014)

Density functional/molecular dynamics simulations with more than 500 atoms have been performed on liquid bismuth at 573, 773, 923, and 1023 K and on neutral Bi clusters with up to 14 atoms. There are similar structural patterns (coordination numbers, bond angles, and ring patterns) in the liquid and the clusters, with significant differences from the rhombohedral crystalline form. We study the details of the structure (structure factor, pair, and cavity distribution functions) and dynamical properties (vibration frequencies, diffusion constants, power spectra), and compare with experimental results where available. While the three short covalent bonds typical to pnictogens are characteristic in both liquid and clusters, the number of large voids and the total cavity volume is much larger in the liquid at 1023 K, with larger local concentration variations. The inclusion of spin-orbit coupling results in a lowering of the cohesive energies in Bi_n clusters of 0.3–0.5 eV/atom. © *2014 AIP Publishing LLC*. [http://dx.doi.org/10.1063/1.4901525]

I. INTRODUCTION

Trends in the structures and other properties of group 15 elements (pnictogens, valence configuration ns^2np^3) have aroused interest for many years.[1] N_2—with a full complement of bonding σ_g- and π_u-orbitals—is the most strongly bound dimer of any element and the constituent of insulating solid nitrogen. The heavier members of the group (P, As, Sb, and Bi) have numerous crystalline forms, most showing a preference for threefold coordination and bond angles near 60° and 90°. White phosphorus is an insulating molecular solid comprising P_4 tetrahedra, and black phosphorus (orthorhombic) can be converted under pressure to the semimetallic A7 structure and—at much higher pressures—to a simple cubic metallic form.[2] Violet P (monoclinic) has cage- and tubelike structures also found in phosphorus clusters. The A7 structure (rhombohedral, $R\bar{3}m$) is the most stable (α-) form of the semimetals As, Sb, and Bi. It comprises puckered layers of atoms with bonds of equal length r_1 (3.072 Å in Bi, bond angle 95°27′) to three neighbors, as well as bonds of length r_2 (3.529 Å in Bi)[1] to three atoms in the next layer. The ratio r_2/r_1 decreases with increasing atomic number,[1] an effect also found in group 16 elements (S, Se, Te, Po) for the ratio of "interchain" to "intrachain" distances.[3,4]

The variety of structural patterns and other properties has made group 15 elements attractive objects of study for decades.[5–7] Eighty years ago, Jones[8,9] explained the high diamagnetism, low (semimetallic) conductivity, and structure of bismuth as a distortion of a simple cubic structure brought about by the existence of a large (Jones) zone containing five valence electrons per atom. This mechanism, often referred to today as a "Peierls instability,"[10] has been invoked in discussions of the structures of group 15 liquids, all of which are characterized by a short-range order similar to that of the underlying A7 structure.[11] Elemental liquids of the heavier members of the group (P to Bi) show unexpected features in the $P - T$ phase diagram, including liquid-liquid phase transitions and variations in the melting curve. At high T and P, phosphorus shows a transition between molecular and polymeric phases.[12,13] Sb and Bi are unusual elements in that the density at the melting point is higher (in Bi by ∼2.8%) than in the crystal at room temperature.

Liquid bismuth has attracted much attention over the past 60 years, due in part to its excellent neutron scattering properties. Although the pair distribution functions show significant scatter,[14] there is clear evidence of a temperature-driven structural phase transition at 1013 K.[15] Inelastic neutron scattering (INS) measurements of the dynamical structure factor $S(Q, \omega)$ near the melting point of Bi show evidence of collective density excitations.[16,17] Bi_n^+ cations[18] have been identified mass spectroscopically to $n > 40$, and photofragmentation of small Bi cluster cations has been observed.[19,20] In addition to measurements on Bi_2 and Bi_4 (in solid Ne and Ar matrices),[21]

a)Present address: ACTA Research Group, Singapore University of Technology and Design, 20 Dover Drive, Singapore 138682.
b)Present address: Abteilung Systeme, Deutsches Klimarechenzentrum, Bundesstraße 45a, D-20146 Hamburg, Germany.
c)Electronic mail: r.jones@fz-juelich.de

on anions Bi_2^-, Bi_3^-, and Bi_4^-,[22] and on jet-cooled Bi_3,[23] it has been found that neutral Bi_n clusters up to $n = 20$ show paramagnetic deflections in Stern-Gerlach experiments for odd n.[24]

Simulations of liquid pnictogens include work on As, Sb, and Bi by Hafner and Jank,[25] who performed molecular dynamics on samples with up to 2000 atoms using an effective pair potential. They showed that the open structures could be interpreted as a modulation of random packing by oscillations in the effective potentials. Ballone and Jones[26] studied the liquid-liquid phase transition in a 4000 atom sample of P using a classical force field fit to an extensive set of density functional (DF) calculations on phosphorus clusters. The first molecular dynamics (MD)/DF simulation of liquid Bi was performed by de Wijs *et al.*[27] on a 60-atom sample over 4.15 ps at 1000 K. Souto *et al.*[28] carried out simulations at 600 K (124 atoms, 600 K, 40 ps, local density approximation for exchange and correlation) and discussed the static and dynamical structure factors, the pair distribution function, and the nature of the collective modes. All of this work has been carried out on simulation samples with 124 or fewer atoms or depends on effective potentials fit to experiment or the results of DF calculations.

$^{209}_{83}$Bi has a half-life for α-decay of 1.9×10^{19} years[29] and is often referred to as the heaviest stable isotope of any element. It has been used frequently to test relativistic effects in molecular and solid state calculations, including wave function based calculations of the dimer[30,31] and trimer.[32] The results of coupled-cluster and density functional calculations have been compared for Bi_3,[33] but almost all recent theoretical work on Bi_n clusters and their ions have used DF methods. The most extensive include Sb_n^- and Bi_n^- to $n = 13$,[34] Bi_n and Bi_n^+ to $n = 24$,[35] Bi_n and Bi_n^- to $n = 13$,[36] Bi_n to $n = 14$,[37] and Bi_n^+ to $n = 14$.[38]

The DF/MD calculations for neutral Bi clusters and liquid Bi described here are the most extensive parameter-free calculations yet performed on either system, and we focus on the structures and dynamical properties. The structures of group 15 elements have been studied in our group for many years. Clusters of phosphorus were among the first where unexpected structures were found using simulated annealing,[39,40] and calculations on clusters of P and As[41] showed that improved cohesive energies resulted when a gradient corrected form[42] of the exchange-correlation energy was used. The polymerization of a liquid comprising P_4 molecules to a disordered network was one of the first phase transitions simulated using DF/MD methods.[43]

II. METHODS OF CALCULATION

A. Density functional calculations

The calculations were performed with the CPMD program[44] using Born-Oppenheimer MD, periodic boundary conditions with a single point ($\mathbf{k} = 0$) in the Brillouin zone, and scalar-relativistic (s-r) Trouiller-Martins pseudopotentials (PP).[45] The cluster calculations used a PP with 15 valence electrons ($5s^{10}6s^26p^3$), a 60 Ry cutoff, and the exchange-correlation functional of Perdew, Burke, and Ernzerhof (PBE).[46] The effect of spin-orbit coupling on the energies of cluster isomers is discussed in Sec. III E. The size of the liquid samples (more than 500 atoms) made some simplifications essential: the PP was constructed for five valence electrons ($6s^26p^3$), with a kinetic energy cutoff of the plane wave basis of 20 Ry. Nonlinear core corrections[47] incorporate the effect of the semicore electrons in the exchange-correlation functional, for which we use the PBEsol approximation.[48] The density cutoff for calculating the gradient corrections was 1.0×10^{-5} in all cases.

The cluster calculations used several strategies to find the most stable Bi_n isomers. Excellent starting structures could be found for $n \leq 10$ by scaling (by $\sim$1.4) the coordinates of low-lying structures of P_n[39,40] and locating the nearest energy minimum. Larger cluster structures were generated by adding atoms to edges or faces of stable clusters or by combining pairs of clusters. Isomers identified in studies by other groups have been tested where appropriate.[35–37] In addition to using simulated annealing and other standard methods for locating energy minima, we generated large numbers of random coordinates for each cluster size and optimized the resulting structures with DF methods. This procedure was carried out up to $n = 20$, but the rapid increase in the number of local energy minima with increasing n means that we have restricted the present analysis to $n \leq 14$. States with the lowest possible multiplicity are generally the most stable, but higher multiplicity states have been checked in most structures with $n < 10$.

Liquid Bi was simulated at four temperatures in cubic simulation boxes with parameters given in Table I. The densities were taken from Ref. 49, the time step was 3.025 fs, and the starting structures were determined from reverse Monte Carlo (RMC) fits to x-ray diffraction data.[50] Equilibration was performed over 10 ps at each temperature before data collection (coordinates r_i and velocities v_i of all atoms). The main focus of the liquid work is on the lowest (573 K) and highest (1023 K) of the four temperatures.

B. Analysis of results

The pair distribution function (PDF) $g(r)$, a spherically averaged distribution of interatomic vectors, can be determined from the atomic coordinates

$$g(r) = \frac{1}{\rho^2}\left\langle \sum_i \sum_{j\neq i} \delta(r_i)\delta(r_j - r)\right\rangle , \qquad (1)$$

where ρ is the atomic number density. The local structure is also characterized by the distributions of the bond angles, the near-neighbor separations, and the ring structures.[51] Cavities (nanosized empty regions) were assigned by using

TABLE I. Simulation parameters.

T (K)	Atoms	Box size (Å)	At. dens. (Å^{-3})	Data coll. (ps)
573	540	26.56103	0.02882	100
773	512	26.30470	0.02813	30
923	512	26.48802	0.02755	30
1023	512	26.61093	0.02717	100

a cubic mesh and determining domains (grid points) that are farther from any atom than a given cutoff (here 2.8 Å) and constructing cells around them according to the Voronoi prescription.[52,53]

The structure factor $S(Q)$ is found by Fourier transformation of $g(r)$:

$$S(Q) = 1 + \rho \int_0^\infty dr\ 4\pi r^2 [g(r) - 1] \frac{\sin(Qr)}{Qr}. \quad (2)$$

The frequency distributions (power spectra) of the liquid phases have been calculated from the Fourier transform of the velocity-velocity autocorrelation function C_v:

$$C_v(t) = \frac{1}{N} \sum_{i=1}^{N} \frac{\langle v_i(0) \cdot v_i(t) \rangle}{\langle v_i(0) \cdot v_i(0) \rangle}, \quad (3)$$

C_v was determined at 573 K and 1023 K from trajectories with 20 000 time steps (over 60 ps). Cluster vibration frequencies were calculated by diagonalizing the dynamical matrix, whose elements are found using finite differences. Vibration frequencies were broadened by a Gaussian of width 1 cm^{-1}. The diffusion constants D were calculated from the coordinates r_i:

$$D = \lim_{t \to \infty} \frac{\langle |r_i(t) - r_i(0)|^2 \rangle}{6t}. \quad (4)$$

III. BISMUTH CLUSTERS Bi_n

Structures, energies, and vibration frequencies have been calculated as described in Sec. II A for numerous isomers of Bi_n clusters up to $n = 14$. Coordinates and relative energies of 58 structures, including those shown in Figs. 1–4, are provided in the supplementary material.[54]

A. Structures

The dimer Bi_2 is the best studied of all Bi clusters, and results of several calculations are compared with experiment in Table II. The DF functional calculations lead to a consistent picture of bond lengths, and the differences in the binding energies reflect in part the use of different approximations for the exchange-correlation energy.

The Bi trimer has two low-lying isosceles triangular (C_{2v}) isomers that are Jahn-Teller distortions of the equilateral triangle structure (D_{3h}). The $^2A_2$ state ($\alpha = 63.9°$, shortest bond $r = 2.91$ Å) is slightly (0.02 eV) more stable than the $^2B_1$ state (56.4°, $r = 2.86$ Å). Similar structures were found by Choi *et al.*,[33] although coupled cluster calculations favor the $^2B_1$ state slightly. The linear structure ($r = 3.04$ Å) and a quartet D_{3h} state with $r = 3.04$ Å lie 1.64 eV and 2.41 eV, respectively, above the $^2A_2$ state. As in the lighter group 15 elements, the most stable tetramer is tetrahedral (T_d, bond length 3.04 Å). The C_{2v} (butterfly) structure is a familiar unit in clusters of P and As and lies 1.58 eV higher in energy than the T_d structure. The bond lengths are 2.98 Å (4 bonds) and 3.19 Å (1).

The two most stable isomers of each of Bi_5, Bi_6, and Bi_7 are shown in Fig. 1. The stability of the structures comprising the butterfly tetramer with an additional atom [5(a)], dimer [6(b)], and trimer [7(a)] is apparent. With the exception of the

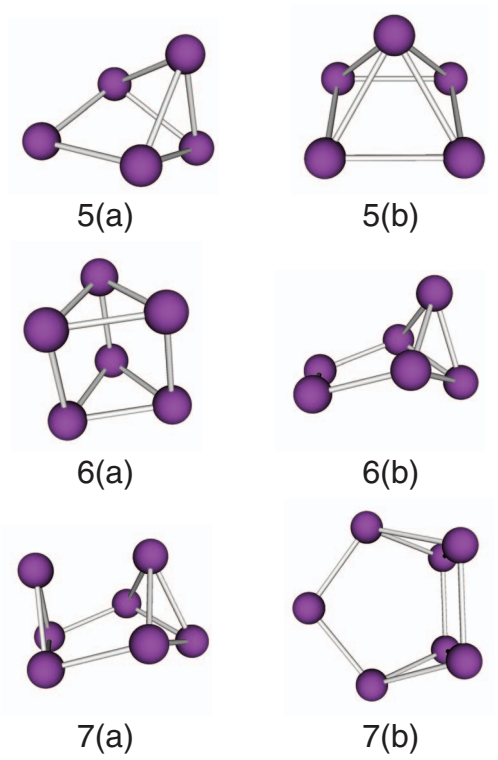

FIG. 1. Isomers of Bi_5, Bi_6, and Bi_7. (a) denotes the most stable isomer, (b) the next highest in energy.

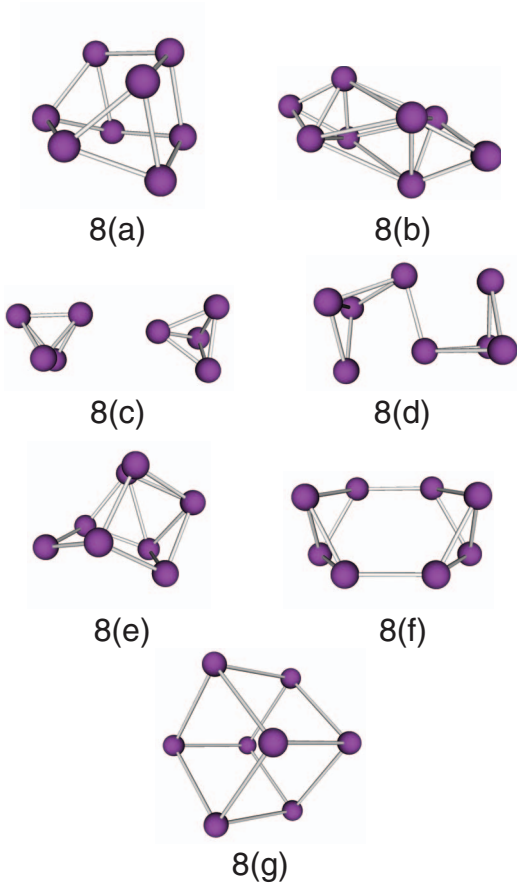

FIG. 2. Isomers of Bi_8, (a)–(e) in order of decreasing stability. The weak "bonds" between the tetrahedra in Bi_8(b) are 4.30 Å long.

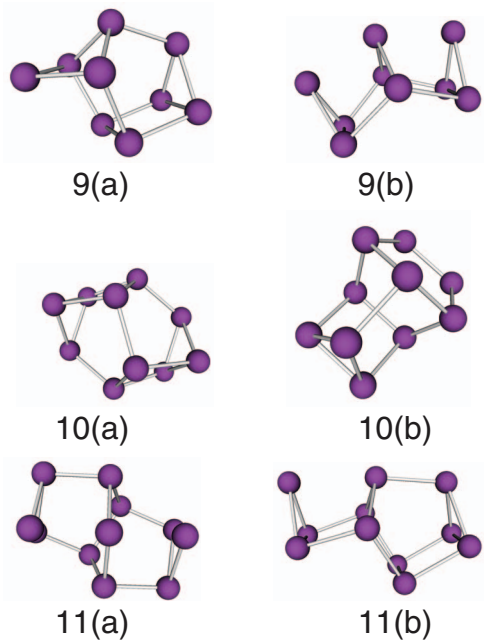

FIG. 3. Isomers of Bi_9, Bi_{10}, and Bi_{11}. (a) denotes the most stable isomer, (b) the next highest in energy.

twofold coordinated dimer atoms (2.83 Å), the bond lengths in these structures lie in a narrow range (3.02–3.10 Å). The longest bonds occur in the C_{4v} isomer of Bi_5 (3.09 Å, 3.15 Å), where the out-of-plane atom is fourfold coordinated. The energies of 7(a) and 7(b) are almost degenerate.

Low-lying isomers of Bi_8 are shown in Fig. 2. Of particular interest is the relative stability of a pair of Bi_4 tetrahedra, which was also found by Hirschfeld and Lustfeld.[57] There are several local minima in the energy surface of the $Bi_4(T_d)$-dimer, but the lowest energy [0.14 eV above (a)] is found when faces of the two tetrahedra (bond lengths 3.04 Å) are

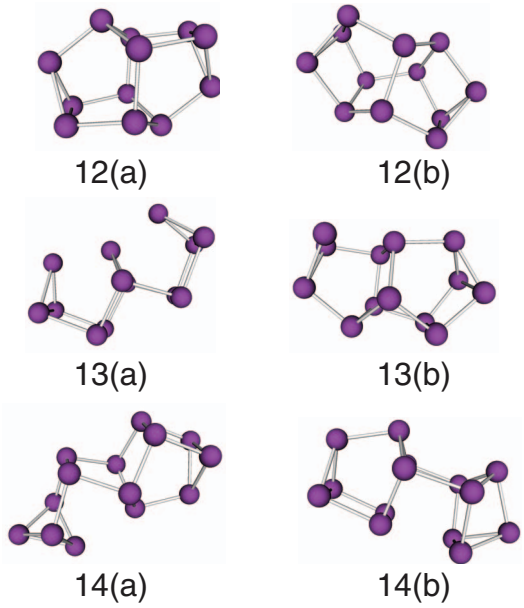

FIG. 4. Isomers of Bi_{12}, Bi_{13}, and Bi_{14}. (a) denotes the most stable isomer, (b) the next highest in energy.

TABLE II. Spectroscopic constants of Bi_2. R-CI: relativistic configuration interaction, DF: density functional.

	r_e (Å)	ω_e (cm^{-1})	E_B (eV)
R-CI[a]	2.76	151	1.88
R-CI[b]	2.734	165	
DF[c]	2.665	182.6	2.75
DF[d]	2.704	184.4	2.18
DF[e]	2.691	190.3	2.48
DF[f]	2.689	192.1	2.61
Expt.[g]	2.6596	172.71	2.1 [h]

[a]Reference 30.
[b]Reference 31.
[c]Reference 36.
[d]Reference 35.
[e]Reference 37.
[f]This work.
[g]Reference 55.
[h]Reference 56.

parallel [8(b)]. The distance between atoms in different tetrahedra is 4.30 Å, and the bonds in the tetrahedra are 3.06 Å. The PBE and other approximation based on the local density approximation for exchange and correlation usually overestimate the strengths of weak bonds between closed shell systems, but the results demonstrate the importance of "clusters of clusters" in group 15 elements. Isomers 8(f) (D_{2h}, with all bonds close to 3.06 Å) and 8(g) (O_h, cube, bond length 3.11 Å) of Bi_8 lie 0.37 eV and 0.47 eV, respectively, above the most stable isomer.

Low-lying isomers of Bi_9 to Bi_{14} are shown in Figs. 3 and 4. Many of these structures can be derived from smaller clusters by adding units with one to four atoms, and structures with higher symmetry, e.g., C_{2h} in Bi_{10}, Bi_{11}, and Bi_{12}, are favored over their lower symmetry counterparts (C_s). Nevertheless, identification of the most stable isomers requires explicit calculation. General remarks on bonding trends are given in Sec. III D.

B. Cohesive energies

In Fig. 5, we show the binding energies per atom (cohesive energy, E_c). The variation of E_c with cluster size follows the pattern found in phosphorus clusters: a general increase with a clear odd-even alternation. The measured enthalpy of vaporization in bulk Bi (2.17 ± 0.02 eV)[58] is also shown. The variation of E_c with n indicates that assemblies of small clusters can have similar energies to more compact clusters with the same total number of atoms.

C. Vibration frequencies

Vibration frequencies for representative isomers of Bi_n clusters are shown in Fig. 6, where frequencies are broadened by a Gaussian function of width 1 cm^{-1}. Previous vibration frequency calculations for clusters with $n > 2$ appear to be limited to the trimer.[33] While the results depend on choice of basis set and effective core potential, the results compare reasonably well with ours. In the $^2A_2$ state, the present calculations give 79, 105, and 160 cm^{-1}, compared with 108 and

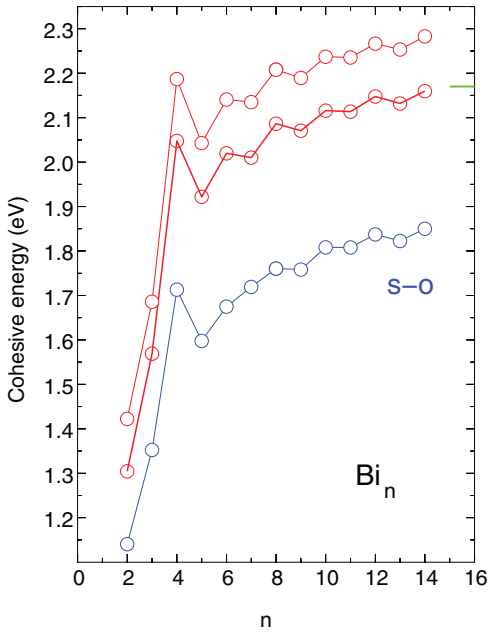

FIG. 5. Cohesive energies of Bi_n clusters for CPMD-optimized geometries. Thick red: CPMD calculations (no s-o coupling), thin red: VASP calculations (no s-o coupling), blue: VASP calculations (s-o coupling), green: experimental cohesive energy of Bi (Ref. 58).

164 cm^{-1} with the B3LYP functional.[33] The corresponding values for the $^2B_1$ state are (89, 121, 166 cm^{-1}) and (124, 173 cm^{-1}), respectively. Our calculations for linear Bi_3 give frequencies of 29, 114, and 171 cm^{-1}.

With the exception of Bi_2, there are few measurements of vibration frequencies in Bi_n clusters. Neon matrix studies of Bi_4[21] show vibration frequencies of 89.8, 120.4, and 149.7 cm^{-1}. Our calculated values (T_d: 93, 120, 122, and 163 cm^{-1}; C_{2v}: 58, 76, 89, 104, 124, and 142 cm^{-1}) support the assignment of the T_d structure as the most stable isomer.

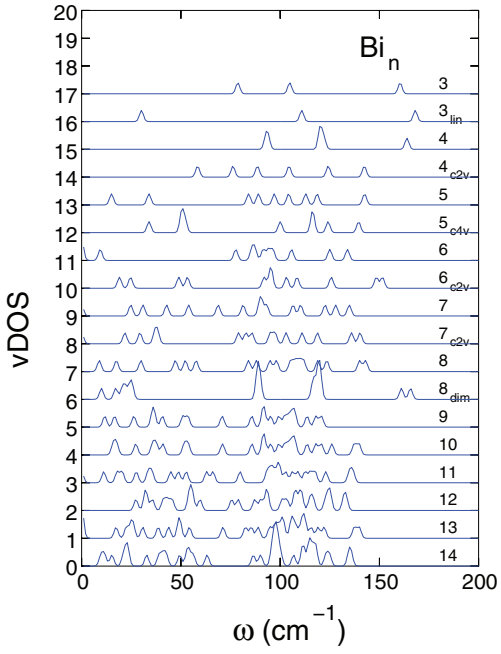

FIG. 6. Vibration densities of states for isomers of Bi_n. Numbers without subscripts denote the most stable isomer.

D. Trends in structures and other properties

There are pronounced similarities between the structures of clusters of group 15 elements, and appropriate scaling of the coordinates for one element is a reliable way of generating starting structures for another. The smallest clusters show a growth pattern based on the C_{2v} (butterfly) isomer of the tetramer, followed by a pattern of disordered pentagonal units for $n = 7$ and tubelike formation in the largest clusters considered here. Most atoms are threefold coordinated, and bond lengths close to the nearest-neighbor separation in the bulk (3.07 Å) are common. Two- and fourfold coordinated atoms do occur, with bonds that are shorter and longer, respectively, than this value. Bond angles in the range 80°–110° are common, but triangular structures lead to bond angles near 60°, which does not occur in the A7 structure of Bi ($\alpha \sim 95.5°$). While the cluster structures show some features of the A7 structure, it is clear that clusters of the size considered here are far from "bulklike" in this respect.

The cohesive energies in Fig. 5, on the other hand, show a rather rapid saturation with increasing n, and the calculated value for Bi_{14} is close to the experimental estimate of the bulk (the effect of spin-orbit coupling is discussed in Sec. III E). The odd-even variation with n is more pronounced than in the group 16 elements sulfur[59] and tellurium[4] and is a direct consequence of the odd number of valence electrons in group 15 elements.

The overall similarity in the structures of clusters of group 15 elements does *not* apply to the relative energies of isomers of a given cluster size. The bonding in Bi clusters is weaker than in P clusters, for example, and the range of isomer energies is much smaller. The energy difference between isomers 8(a) and 8(g) in Fig. 2 is 0.47 eV in Bi, but over 1.7 eV in P. Even more striking is that the $P_4(T_d)$-dimer is the most stable form of P_8 (by ∼0.4 eV, see also Ref. 57), while in Bi it is over 0.1 eV less stable than 8(a).

The vibration frequencies (Fig. 6) cover the range of phonon frequencies measured in crystalline Bi [74–108 cm^{-1}, INS at 300 K;[60] 66 cm^{-1} (A_{1g}), 92.5 cm^{-1} (E_g), $k = 0$ Raman spectra at 500 K (Ref. 61)]. Twofold coordinated atoms in the clusters have higher frequencies. The frequencies of the $Bi_4(T_d)$-dimer are related to those of most stable $Bi_4(T_d)$ form, supplemented by low-frequency vibrations corresponding to the weak bonds between the groups.

E. Effect of spin-orbit coupling

Relativistic effects[62] must be included in calculations involving heavy elements, and Bi ($Z = 83$) is no exception. The relativistic generalization of the Kohn-Sham equations incorporates the mass-velocity, Darwin, and spin-orbit terms, the first two of which are spin-independent and are numerically the largest in most atoms. Mass-velocity, Darwin, and the average of spin-orbit components make up the "scalar

relativistic" approximation we use to construct the pseudopotential of Bi. Nevertheless, spin-orbit interactions are particularly important in heavy elements with a partially filled *p*-shell, such as Bi or Pb ($Z = 82$). Spin-orbit interactions *reduce* the dissociation energy of the Pb dimer.[63]

The CPMD program used in the simulations of liquid Bi and the cluster calculations described above does not incorporate spin-orbit coupling, and we have used the VASP program[64] to check its effect on cluster energetics. We used the PBE exchange-correlation energy functional, as in the CPMD calculations, a projected augmented wave (PAW) pseudopotential for Bi with 15 valence electrons, and an energy cutoff of 500 eV. The first main effect of spin-orbit coupling is the stabilization of the $6p^3$ ($^4S^0_{3/2}$) ground state of the atom. This is evident in the Bi_2 dimer, where the bond length is increased from 2.652 Å to 2.681 Å. The dissociation energy is reduced from 2.84 eV to 2.28 eV (0.28 eV/atom) and is closer to the experimental estimate (2.1 eV).[56] The presence of significant spin-orbit coupling mixes all configurations that have the same symmetry in the spin double group, and this is consistent with the lower dissociation energies and the smaller HOMO-LUMO gaps found in all these clusters. It can also lead to a quenching of Jahn-Teller splittings found in scalar relativistic calculations.[32,65] In Bi_3, spin-orbit calculations for the equilateral triangular structure lead to a bond length of 2.96 Å and a cohesive energy of 1.35 eV.

The effect of spin-orbit coupling has been tested on larger clusters by two sets of energy calculations for the geometries determined by our s-r calculations. First, spin-polarized, s-r calculations were performed for direct comparison, followed by the addition of the spin-orbit coupling potential. The components of the forces on the nuclei were calculated to ensure that the structure was in the neighborhood of the energy minimum. The s-r calculations with VASP led to cohesive energies that were uniformly between 0.1 and 0.15 eV/atom higher than the CPMD results (see Fig. 5), reflecting the different programs and pseudopotential constructions. Spin-orbit coupling lowers the cohesive energy by between 0.4 and 0.5 eV/atom, and the variation with n is remarkably uniform, with the exception of the spin-orbit value for Bi_6. This last result probably reflects the use of the s-r structure without further optimization.

The energy differences between isomers of a given cluster are much smaller than the differences in cohesive energies (the energies given in the supplementary material[54] are for the *cluster*, not eV/atom), but spin-orbit coupling changes the ordering of isomer stability in few cases. There are significant exceptions: In Bi_6 and Bi_{10}, the (b) isomer is more stable than the (a) isomer, in Bi_9 the (a) isomer remains the most stable, but the (b) and (c) isomers change places. The most surprising change is the increased stability of Bi_8 isomer (e) with respect to all others, since structures involving fourfold coordinated atoms seldom belong to the most stable isomers of group 15 elements. The use of the original (CPMD) coordinates without further optimization is a source of uncertainty, and a thorough study of the role of spin-orbit coupling in Bi clusters would be welcomed. The structures provided in the supplementary material[54] should be useful in this context.

IV. LIQUID BISMUTH

A. Structure factor, pair distribution function, and near-neighbor separations

Snapshots of the liquid samples at 573 K and 1023 K are shown in Fig. 7, and in Fig. 8(a) we show the PDFs and in Fig. 8(b) structure factors $S(Q)$ for the liquid at all four temperatures. The first PDF peak that usually corresponds to chemical (covalent) bonds is extended up to 4.0 Å followed by a shoulder. This feature is much broader than for lighter pnictogens (in particular Sb), and the absence of a well-defined first minimum complicates the analysis of coordination numbers. Also shown are the experimental (ND) results of Greenberg *et al.*[15] The calculations reproduce the weak shoulder in $S(Q)$ on the high-Q side of the first peak. Although the temperatures of the two sets of data are not identical, the agreement between theory and experiment is very encouraging.

The distribution of separations of up to the 12 nearest neighbors (Fig. 9) shows interesting features. While bonds to the more distant neighbors expand steadily as the temperature increases, there is little change in the distance to the first three neighbors. The maxima of the nearest neighbor distributions at all temperatures (3.06–3.08 Å) are close to the nearest neighbor separation in crystalline Bi (3.072 Å) and the most common bond length in the clusters (3.06 Å). Furthermore, distributions 4–6 are still below 4.0 Å and show a smaller shift and narrower distributions than more distant neighbors (7–12).

To avoid ambiguities arising from the broad first peak in the PDF, we have employed the effective coordination number (ECN),[66] where the average value of bond distances is calculated iteratively for each atom and the bonds are weighted accordingly. The ECN values are 6.84 (573 K) and 6.07 (1023 K), and the distributions are shown in the supplementary material.[54] These values correspond to cutoff distances of 3.82 and 3.79 Å for standard PDF integrations over the first peak. The density of the liquid at 573 K is higher than in the bulk $A7$ structure ($N = 6$), but becomes lower at higher temperatures, reverting to sixfold effective coordination at 1023 K.

B. Bond angle distributions

The bond angle distribution at 573 K is shown in Fig. 10. The dependence of the distribution depends on the

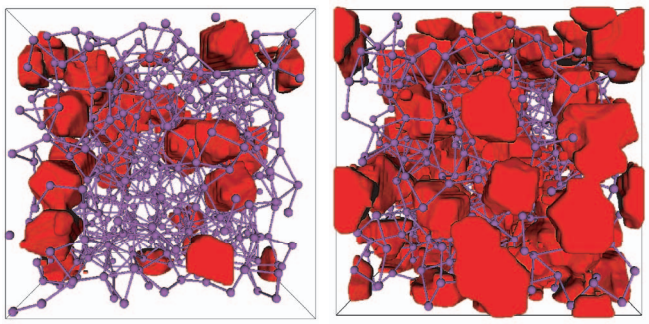

FIG. 7. Snapshots of liquid Bi at (a) 573 K and (b) 1023 K. The cavities are shown in red.

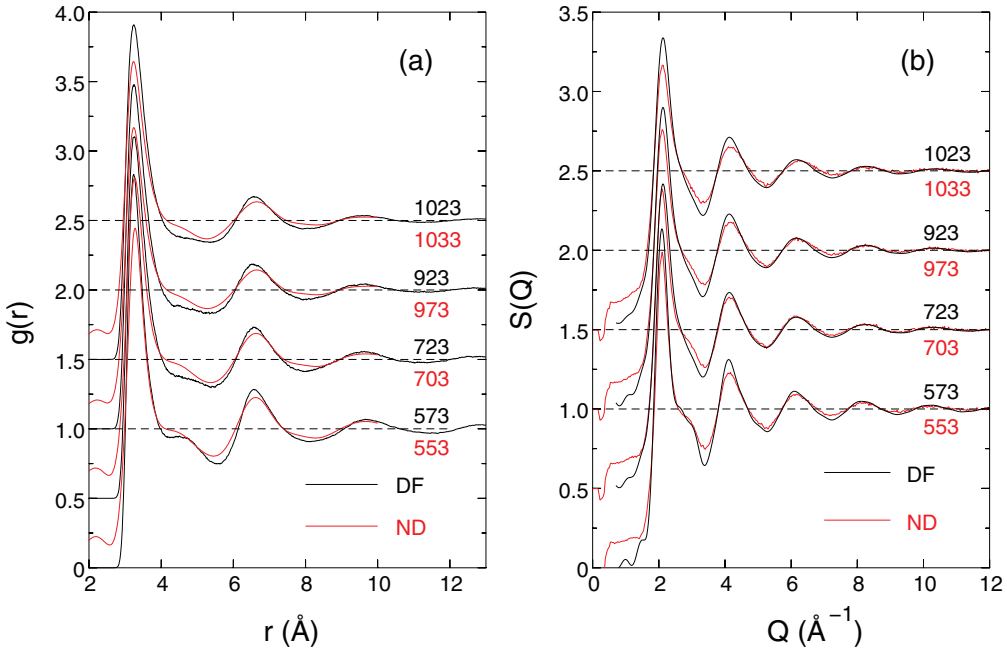

FIG. 8. (a) Pair distribution functions for liquid Bi at the temperatures shown. Black: present calculations, red: neutron scattering data (Ref. 15). (b) Corresponding structure factors.

cutoff distance used to define a "bond," so we have calculated the bond angle distribution for four cutoffs. Figure 10 shows that a preference for octahedral orientation at low radii shifts gradually towards 60° at longer radii. The distributions at 1023 K (see the supplementary material)[54] are similar, but weaker and broader. The importance of triangular configurations (∼60°) even for the shortest bond cutoff (3.5 Å) emphasizes the angular disorder.

C. Rings and cavities

Rings and cavities are analyzed as described above (Sec. II B). Simulations of hundreds of atoms are needed to avoid distortions caused by periodic boundary conditions. The distribution of rings (closed paths along bonds) is shown in Fig. 11 for 573 K (cutoff 3.82 Å) and 1023 K (cutoff 3.79 Å). Rings with three or four atoms are the most common, and there is more weight for larger rings at the higher temperature. These changes reflect the reduced coordination and atomic density at high *T*.

Cavities are characteristic of liquid Bi, and the analysis was performed using a test sphere radius of 2.8 Å and a grid spacing of 0.057 Å. Figure 12 shows the distribution of the cavity volumes, i.e., the sum of the volumes of the cavities in a certain size range. The differences between the two temperatures are significant: At 573 K, the cavity volume comes from relatively small cavities, but there are large multicavities at 1023 K that span the simulation cell (26.6 Å). The total cavity volumes on average are 931 Å^3 (4.96% of total) at 573 K, 3486 Å^3 (18.50%) at 1023 K. The change in the cavity volumes is also reflected in the systematic shift of the

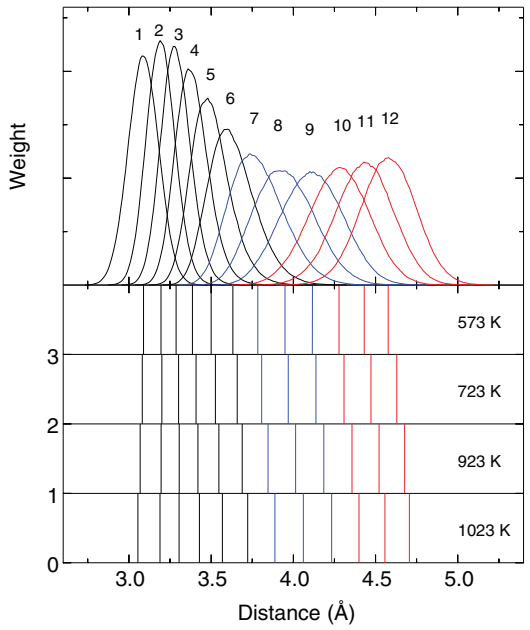

FIG. 9. Near-neighbor distributions in liquid Bi at 573 K. Below are shown the average distances of each neighbor at all four simulation temperatures.

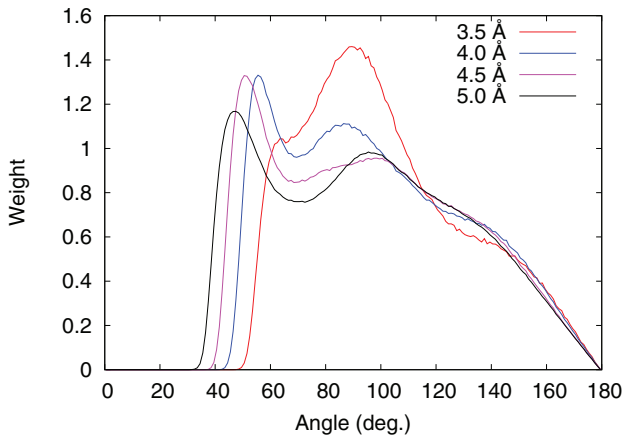

FIG. 10. Bond angle distribution at 573 K as a function of cutoff distance.

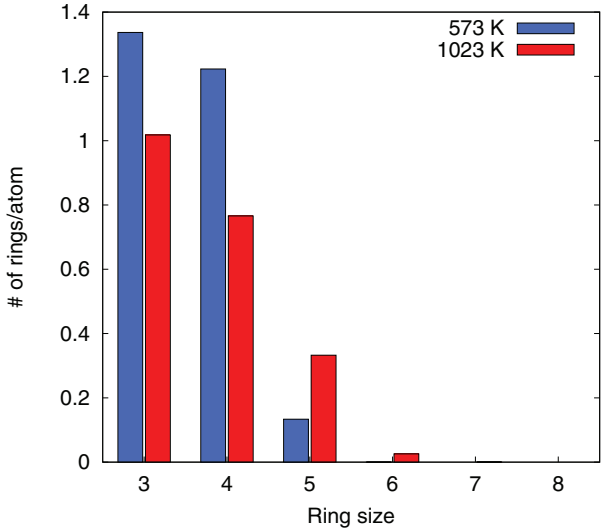

FIG. 11. Ring distributions in liquid Bi at 573 and 1023 K.

near-neighbor distributions 7–12 (Fig. 9) which correspond to distances on the second coordination shell (non-bonded atoms).

D. Dynamics

The diffusion constants for the four temperatures (Eq. (4)) are given in Table III. A linear relationship between $\log D$ and $1/T$ gives an activation barrier of 0.126 eV for self-diffusion in liquid Bi. The value of D at 573 K is consistent with earlier DF/MD calculations at 600 K ($1.91 \pm 0.05 \times 10^{-5}$cm^2/s)[28] and the interpolation formula based on tracer diffusion experiments (1.74×10^{-5}cm^2/s),[67] although the error bars in the latter are large (~30%).

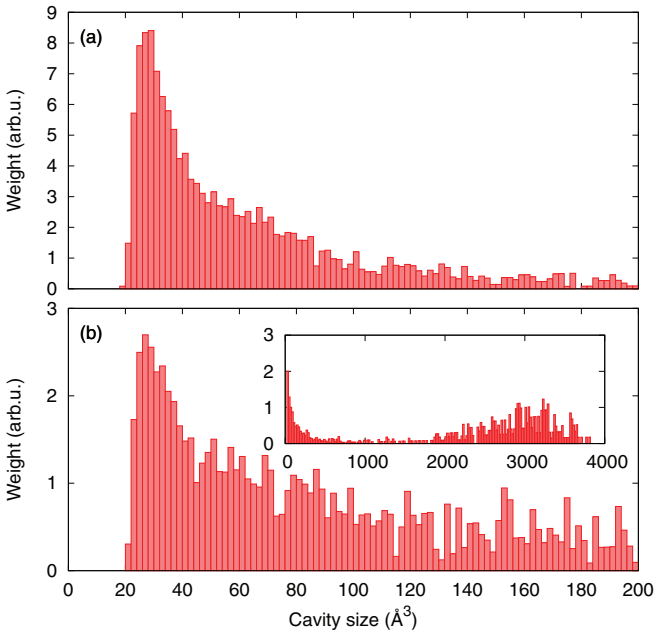

FIG. 12. Distribution of cavity volumes in Bi at (a) 573 K and (b) 1023 K. The panels have the same units. Inset: Large cavities at 1023 K.

TABLE III. Self-diffusion constant D (10^{-5} cm^2/s) of Bi at temperatures T (K).

T	573	773	923	1023
D	1.81	3.28	4.90	5.47

The power spectra (vibrational densities of states) are shown in Fig. 13 for liquid Bi at 573 and 1023 K. There is a broad peak at ~65 cm^{-1} at both temperatures, with frequencies similar to the range found in optical phonons in crystalline Bi, and a second peak (~15 cm^{-1}) at 573 K. A two-peak structure was found at similar energies in the simulations at 600 K of Souto *et al.*[28] It is remarkable that the ~65 cm^{-1} peak exists also at 1023 K although the temperature is ~480° above the melting point. The tail of the distribution above ~100 cm^{-1} arises from bond stretching modes that are also apparent in Bi$_n$ clusters in Fig. 6. A detailed analysis of the collective density excitations is in progress, and the results will be presented elsewhere.

E. Electronic structure

The general features of the electronic band structure of crystalline Bi are both well known[68] and consistent with x-ray photoemission spectroscopy on amorphous and crystalline Bi.[69] The three bands near the Fermi energy arising from 6*p*-electrons have antibonding, lone-pair, and bonding components and are separated by ~4 eV from two bands at lower energies arising from the 6*s*-electrons. The Kohn-Sham eigenvalue spectra (electronic density of states, DOS) for 573 K and 1023 K are shown in Fig. 14. The overall picture is similar to that in amorphous and crystalline Bi, with two broad bands from the Fermi energy to −4 eV, and between −8 and −12 eV. The non-zero density of states at the Fermi energy is consistent with the metallic behavior of Bi at these temperatures.

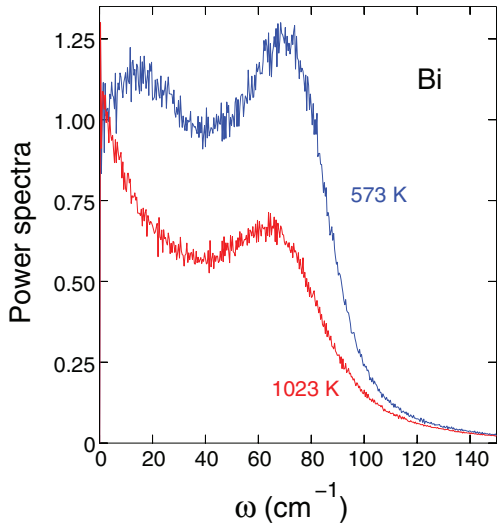

FIG. 13. Calculated power spectra for liquid Bi at 573 K (blue) and 1023 K (red). Curves are normalized to unity at zero frequency.

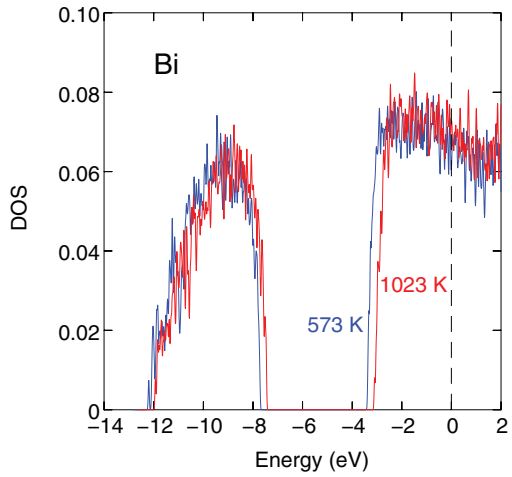

FIG. 14. Electronic density of states for liquid Bi at $T = 573$ K (blue) and 1023 K (red). The Fermi energy (dashed) is zero in each case.

V. DISCUSSION AND CONCLUDING REMARKS

Combined density functional/molecular dynamics calculations have been performed on neutral Bi_n clusters ($n = 2$–14) and on liquid Bi at 573, 773, 923, and 1023 K with over 500 atoms in the unit cell. They are the most extensive DF simulations performed to date on either system, and we have focused on the structures and vibrational properties.

Bismuth clusters show similar structural patterns (including coordination numbers, bond angles, ring patterns, etc.) to those found in clusters of lighter group 15 elements. While these patterns are particularly evident in allotropes of P, this is not true in Bi, where the most stable (rhombohedral) form is a modest distortion of a simple cubic structure comprising threefold coordinated atoms. The energy differences between different isomers, and the energy barriers between them, are much less in Bi_n clusters than in the corresponding clusters of P and As. In terms of structural patterns, liquid Bi and Bi clusters are more similar to each other than to the crystalline A7 structure. The density of liquid Bi decreases between 573 K and 1023 K, and cavities become more important (5% of the total volume to 18.5%). This change is associated with the reduction of the effective coordination number from 6.84 to 6.07 as T increases.

The structural variety in Bi clusters is reflected in the range of vibration frequencies up to ~150 cm^{-1}. The power spectrum of the liquid shows a broad peak near 70 cm^{-1} at 573 K and 1023 K, as well as a weaker peak near 15 cm^{-1} at the lower temperature.

ACKNOWLEDGMENTS

We acknowledge gratefully the computer time provided by the JARA-HPC Vergabegremium on the JARA-HPC partition of the supercomputer JUQUEEN at Forschungszentrum Jülich, and for time granted on the supercomputer JUROPA at Jülich Supercomputer Centre. We thank S. Kohara for providing starting geometries based on reverse Monte Carlo analysis of x-ray diffraction data, and G. Makov and colleagues for providing their original ND data. J.A. acknowledges financial support from the Academy of Finland through its Centres of Excellence Program (Project 251748). The German Research School for Simulation Sciences is a joint venture of the FZ Jülich and RWTH Aachen University.

[1] J. Donohue, *The Structures of the Elements* (Wiley, New York, 1974), Chap. 8.
[2] J. C. Jamieson, Science **139**, 1291 (1963).
[3] J. Akola, R. O. Jones, S. Kohara, T. Usuki, and E. Bychkov, Phys. Rev. B **81**, 094202 (2010).
[4] J. Akola and R. O. Jones, Phys. Rev. B **85**, 134103 (2012).
[5] J. K. Burdett and S. Lee, J. Solid State Chem. **44**, 415 (1982).
[6] X. Gonze, J.-P. Michenaud, and J.-P. Vigneron, Phys. Rev. B **41**, 11827 (1990).
[7] S. E. Boulfelfel, G. Seifert, Y. Grin, and S. Leoni, Phys. Rev. B **85**, 014110 (2012).
[8] H. Jones, Proc. Phys. Soc., London, Sect. A **147**, 396 (1934).
[9] N. F. Mott and H. Jones, *The Theory of the Properties of Metals and Alloys* (Clarendon Press, Oxford, 1936), p. 166.
[10] R. Peierls, *Quantum Theory of Solids* (Clarendon Press, Oxford, 1955), p. 108.
[11] M. Mayo, E. Yahel, Y. Greenberg, and G. Makov, J. Phys.: Condens. Matter **25**, 505102 (2013), and references therein.
[12] Y. Katayama, T. Mizutani, W. Utsumi, O. Shinomura, M. Yamakata, and K. Funakoshi, Nature (London) **403**, 170 (2000).
[13] G. Monaco, S. Falconi, W. A. Crichton, and M. Mezouar, Phys. Rev. Lett. **90**, 255701 (2003).
[14] M. Mayo, E. Yahel, Y. Greenberg, E. N. Caspi, B. Beuneu, and G. Makov, J. Appl. Crystallogr. **46**, 1582 (2013).
[15] Y. Greenberg, E. Yahel, E. N. Caspi, C. Benmore, B. Beuneu, M. P. Dariel, and G. Makov, Europhys. Lett. **86**, 36004 (2009).
[16] K. Shibata, S. Hoshino, and H. Fujishita, J. Phys. Soc. Jpn. **53**, 899 (1984).
[17] L. Sani, L. E. Bove, C. Petrillo, and F. Sacchetti, J. Non-Cryst. Solids **353**, 3139 (2007), and references therein.
[18] T. M. Bernhardt, B. Kaiser, and K. Rademann, Phys. Chem. Chem. Phys. **4**, 1192 (2002).
[19] M. E. Geusic, R. R. Freeman, and M. A. Duncan, J. Chem. Phys. **88**, 163 (1988).
[20] M. M. Ross and S. W. McElvany, J. Chem. Phys. **89**, 4821 (1988).
[21] V. E. Bondybey and J. H. English, J. Chem. Phys. **73**, 42 (1980), and references therein.
[22] M. L. Polak, J. Ho, G. Gerber, and W. C. Lineberger, J. Chem. Phys. **95**, 3053 (1991).
[23] C. A. Arrington and M. D. Morse, J. Phys. Chem. B **112**, 16182 (2008).
[24] S. Yin, X. Xu, R. Moro, and W. A. de Heer, Phys. Rev. B **72**, 174410 (2005).
[25] J. Hafner and W. Jank, Phys. Rev. B **45**, 2739 (1992).
[26] P. Ballone and R. O. Jones, J. Chem. Phys. **121**, 8147 (2004).
[27] G. A. de Wijs, G. Pastore, A. Selloni, and W. van der Lugt, Phys. Rev. Lett. **75**, 4480 (1995).
[28] J. Souto, M. M. G. Alemany, L. J. Gallego, L. E. González, and D. J. González, Phys. Rev. B **81**, 134201 (2010).
[29] P. de Marcillac, N. Coron, G. Dambier, J. Leblanc, and J.-P. Moalic, Nature (London) **422**, 876 (2003).
[30] K. Balasubramanian and D.-W. Liao, J. Chem. Phys. **95**, 3064 (1991).
[31] K. K. Das, H.-P. Liebermann, R. J. Buenker, and G. Hirsch, J. Chem. Phys. **102**, 4518 (1995).
[32] K. Balasubramanian, K. Sumathi, and D. Dai, J. Chem. Phys. **95**, 3494 (1991).
[33] H. Choi, C. Park, and K. K. Baeck, J. Phys. Chem. A **106**, 5177 (2002).
[34] M. Gausa, R. Kaschner, G. Seifert, J. H. Faehrmann, H. O. Lutz, and K.-H. Meiwes-Broer, J. Chem. Phys. **104**, 9719 (1996).
[35] H. K. Yuan, H. Chen, A. L. Kuang, Y. Miao, and Z. H. Xiong, J. Chem. Phys. **128**, 094305 (2008).
[36] L. Giao, P. Li, H. Lu, S. F. Li, and Z. X. Guo, J. Chem. Phys. **128**, 194304 (2008).
[37] J. M. Jia, G. B. Chen, D. N. Shi, and B. L. Wang, Eur. Phys. J. D **47**, 359 (2008).
[38] R. Kelting, A. Baldes, U. Schwarz, T. Rapps, D. Schooss, P. Weis, C. Neiss, F. Weigend, and M. M. Kappes, J. Chem. Phys. **136**, 154309 (2012).
[39] R. O. Jones and D. Hohl, J. Chem. Phys. **92**, 6710 (1990).
[40] R. O. Jones and G. Seifert, J. Chem. Phys. **96**, 7564 (1992).
[41] P. Ballone and R. O. Jones, J. Chem. Phys. **100**, 4941 (1994).

[42]J. P. Perdew, Phys. Rev. B **33**, 8822 (1986); A. D. Becke, Phys. Rev. A **38**, 3098 (1988).
[43]D. Hohl and R. O. Jones, Phys. Rev. B **50**, 17047 (1994).
[44]CPMD V3.15 ©IBM Corp 1990–2011, ©MPI für Festkörperforschung Stuttgart 1997–2001, see http://www.cpmd.org.
[45]N. Troullier and J. L. Martins, Phys. Rev. B **43**, 1993 (1991).
[46]J. P. Perdew, K. Burke, and M. Ernzerhof, Phys. Rev. Lett. **77**, 3865 (1996).
[47]S. G. Louie, S. Froyen, and M. L. Cohen, Phys. Rev. B **26**, 1738 (1982).
[48]J. P. Perdew, A. Ruzsinszky, G. I. Csonka, O. A. Vydrov, G. E. Scuseria, L. A. Constantin, X. Zhou, and K. Burke, Phys. Rev. Lett. **100**, 136406 (2008).
[49]M. J. Assael, A. E. Kalyva, K. D. Antoniadis, R. M. Banish, I. Egry, J. Wu, E. Kaschnitz, and W. A. Wakeham, High Temp. – High Pressures **41**, 161 (2012).
[50]S. Kohara, private communication (2011).
[51]ISAACS program, S. Le Roux and V. Petkov, J. Appl. Crystallgr. **43**, 181 (2010).
[52]J. Akola and R. O. Jones, Phys. Rev. B **76**, 235201 (2007).
[53]J. Akola and R. O. Jones, Phys. Rev. Lett. **100**, 205502 (2008).
[54]See supplementary material at http://dx.doi.org/10.1063/1.4901525 for figures of 33 structures not shown here, coordinates of all 58 structures, the distributions of bond angles (at 1023 K), and effective coordination numbers (573 K and 1023 K).
[55]G. Gerber and H. P. Broida, J. Chem. Phys. **64**, 3423 (1976).
[56]F. J. Kohl, O. M. Uy, and K. D. Carlson, J. Chem. Phys. **47**, 2667 (1967).
[57]J. Hirschfeld and H. Lustfeld, Phys. Rev. E **85**, 056709 (2012).
[58]Cohesive energy from R. Hultgren, P. D. Desai, D. T. Hawkins, M. Gleiser, K. K. Kelley, and D. G. Wagman, *Selected Values of the Thermodynamic Properties of the Elements* (American Society for Metals, Metals Park, OH, 1973), p. 73.
[59]R. O. Jones and P. Ballone, J. Chem. Phys. **118**, 9257 (2003).
[60]J. L. Yarnell, J. L. Warren, R. G. Wenzel, and S. H. König, IBM J. Res. Dev. **8**, 234 (1964).
[61]J. Höhne, U. Wenning, H. Schulz, and S. Hüfner, Z. Phys. B **27**, 297 (1977).
[62]See, for example, K. Balasubramanian and K. S. Pitzer, in *Ab Initio Methods in Quantum Chemistry. I*, Advances in Chemical Physics, edited by K. P. Lawley (Wiley, New York, 1987), Vol. 67, p. 287.
[63]K. Balasubramanian and K. S. Pitzer, J. Chem. Phys. **78**, 321 (1983).
[64]G. Kresse and J. Furthmüller, Phys. Rev. B **54**, 11169 (1996).
[65]K. Balasubramanian, Mol. Phys. **107**, 797 (2009).
[66]J. L. F. Da Silva, J. Appl. Phys. **109**, 023502 (2011).
[67]See, for example, G. Döge, Z. Naturforsch. A **20**, 634 (1965).
[68] See, for example, X. Gonze, J.-P. Michenaud, and J.-P. Vigneron, Phys. Scr. **37**, 785 (1988).
[69]L. Ley, R. A. Pollak, S. P. Kowalczyk, R. McFeely, and D. A. Shirley, Phys. Rev. B **8**, 641 (1973).